Menghua Lu[1]
Lijuan Zhang[1,*]
Jiayi Li[1]
Jie Lu[1]
Fengjiao Liu[1]
Jos J. Derksen[2]

Experiments on and Simulations of Hollow Cylinders Falling through Quiescent Liquids

Quantitative visualization experiments of hollow cylinders falling through a Newtonian liquid were performed. The Archimedes number was in the range 5 to 10^5, the length/outer diameter ratio of the cylinders was in the range 2.5–10, and the inner/outer diameter ratio was 0–0.85. The definition of the Archimedes number includes the inner and outer cylinder diameters, and it is shown that cylinders with the same Archimedes number having different diameter ratios behave similarly. Particle-resolved simulations were used to enhance the insight into the fluid flow generated by the settling cylinder. They were also used to assess the flow through a hollow cylinder during settling.

Keywords: Nonspherical particles, Particle-resolved simulation, Quantitative visualization, Sedimentation

Received: June 14, 2023; *revised:* October 19, 2023; *accepted:* November 23, 2023

DOI: 10.1002/ceat.202300285

Supporting Information available online

1 Introduction

We study sedimentation of a rigid, hollow, cylindrical particle through a liquid. There are a number of reasons to study a relatively simple system such as this. Some reasons directly relate to practical applications, mostly in chemical engineering. Other reasons relate to the development and improvement of modeling of the dynamical behavior of nonspherical particles in fluids, with such modeling having practical importance over a broad range of technological applications.

In various branches of engineering, one encounters solid particles suspended in a fluid. In civil and environmental engineering these include dredging [1], sediment transport in rivers and coastal areas [2], and wastewater treatment. In chemical engineering, fluidization and catalytic slurry reactors are used for (reactive) mass transfer between solids and fluids. An application in petroleum engineering is transport of drilling mud (drilling fluid laden with rock cuttings). In modeling such systems and processes, the shape of the solids is often not explicitly considered and particles are implicitly assumed to be spherical. For example, two-fluid models as part of multiphase computational fluid dynamics solvers use correlations for drag on spherical particles to account for fluid-solids interaction [3]. Whereas the assumption of spherical shape is reasonable for, e.g., sand grains and fluid catalytic cracking powders, there are situations in which particles deviate so strongly from the spherical form that their shape significantly influences their individual and collective behavior. The processing of biomass is a prominent example [4]. Biomass is a dense suspension containing fibrous solid material that is notoriously difficult to transport and convert [5]. Particles of cylindrical shape are also contained in the thick slurries from which Li-ion battery electrodes are produced [6]. Hollow (cylindrical) particles have the potential for transfer enhancement as a result of the additional surface area of their pore(s). Specific particle shapes have been designed that optimize mass and heat transfer processes in fixed- and fluidized-bed reactors [7–9].

Particularly for sedimentation, the shape of particles is a decisive factor in how sedimentation processes evolve. In 1969, Strinham et al. [10] studied the settling behavior of disks, cylinders, oblate and prolate spheroids, and spheres falling in a quiescent liquid, including the particle's orientation, settling speed, and the path traveled. It was concluded that the stability of falling particles is related to the stability of the pressure distribution in the wake of the particle. Komar et al. [11] investigated the influence of particle shape on drag coefficient and settling speed. They used ellipsoidal pebbles falling through glycerol. They interpreted their results in terms of a sphericity shape factor that allows for the estimation of drag coefficients of nonspherical grains. More recently, the motion of freely falling cylinders in a low-viscosity fluid was experimentally studied by Toupoint et al. [12]. The influence of the Archimedes number (200–1100) and the length/diameter aspect ratio (2–20) on the settlement path of the cylinder was reported.

This paper reports on experiments on hollow cylinders settling in a Newtonian liquid. Through quantitative visualization it was measured how their settling speed and orientation evolve over time starting from vertical release. The effects of

[1]Menghua Lu, Prof. Lijuan Zhang (zhanglj0128@126.com), Jiayi Li, Prof. Jie Lu, Fengjiao Liu
School of Chemistry and Chemical Engineering, Shanghai University of Engineering Science, 333 Longteng Road, Songjiang District, 201600, Shanghai, China.

[2]Dr. Jos J. Derksen
School of Engineering, University of Aberdeen, Regent Walk, Aberdeen AB24 3FX, United Kingdom.

the length/outer diameter aspect ratio and the outer/inner diameter ratio of the cylinders were investigated. By varying the size of the cylinders and the liquid viscosity, it was possible to cover a wide range of Archimedes numbers.

The experiments are supported by numerical simulations that explicitly account for the hollow cylinder shape. One aim of the experiments reported herein was to establish a database that can be used for validating simulation work, and it is shown here what such validation could look like. Also, the simulations provide additional insights, such as the structure of the liquid flow field induced by the sedimenting particle and the strength of the flow through the cylinder's inner diameter. As discussed above, the latter has potential relevance for applications involving mass transfer. Vice versa, the experimental results were used to assess the quality of the predictions made by the simulations and thus to validate the inevitable assumptions and approximations made in designing and executing the simulation procedure.

Our numerical simulations attempt to resolve the flow around and through the settling hollow cylinders, i.e., they represent the shape of the particle by solving the flow on a mesh that is finer by one order of magnitude than the outer diameter of the cylinder and explicitly apply no-slip at the solid surfaces. Such particle-resolved simulations (PRSs) are a relatively recent development [13], initially used for flow around moving spheres [14]. PRSs of sedimenting nonspherical particles have been reported by Wachs et al [15], and PRSs of fluidization of cylindrical particles by Derksen [16].

This paper builds upon our previous experimental and numerical work on the settling of solid cylinders [17], where it was shown that the Archimedes number is the principal parameter that determines the sedimentation process, both in terms of settling speed and the evolution of the cylinder's orientation. The current paper extends this work by adding the inner diameter as an additional degree of freedom. By careful choice of the definition of the Archimedes number for hollow cylinders it is possible to have a common framework for settling of solid and hollow cylinders.

This paper is organized along the following lines. Sects. 2–4 present the experimental methods, dimensional analysis, and numerical methods. The dimensionless numbers that govern the flow system, most importantly the Archimedes number, are defined and the ranges over which they were varied are discussed. Sect. 5 first shows visualizations of cylinder settling and impressions of the simulations. The visualizations are quantified in terms of cylinder orientation angle and settling speed. Experiments and simulations are compared in terms of these quantities and the way in which they depend on the Archimedes number and on cylinder aspect ratios. Sect. 6 summarizes, reiterates the main conclusions, and looks forward to future work.

2 Experimental Setup

The settling column has a square 80 mm × 80 mm footprint and is 800 mm high. It has transparent acrylic side walls. It is filled with a glycerol-water mixture, which is a clear, Newtonian liquid. The ratio of the two components determines the viscosity and density of the mixture. The temperature of the system was maintained at 25±1 °C.

A total of 36 cylindrical particles were utilized in the experiment, most of them hollow. They are all made of stainless steel (ρ_s = 8.04 g cm^{-3}). They have lengths ranging from l = 1.00 to 29.20 mm, outer diameters ranging from d_o = 1.00 to 2.99 mm, and inner diameters ranging from d_i = 0 (solid cylinder) to 1.70 mm. The mass of each cylinder was measured with an electronic balance with an accuracy of ± 0.01 mg. The measurement error of cylinder diameter and length is 0.05 mm.

At the start of an experiment, the cylindrical particle was completely immersed in the liquid before being released, ensuring that the hollow space of the cylinder was completely filled with the glycerol-water mixture. Tweezers were used to hold one end of the vertically oriented cylinder while it was slowly lowered into the liquid near the center of the cross section of the settling column. When the liquid surface was free of ripples, the tweezers were loosened and the particle was let go with the cylinder vertical within an angle of ± 0.5°.

The settling of the cylinder was filmed with a digital camera. It has a resolution of 1920 × 1080 pixels and can be operated with variable frame rate f. The frame rate of the camera was adjusted according to the settling speed. Given the frame rate, the position of the center of gravity of the cylinder can be determined as a function of time. Each pixel represents a square with side length δ = 0.77±0.01 mm in the liquid column. The particle diameter is less than 4 % of the lateral length of the settling column so that, at least during the initial vertical stage of settling, the effect of the walls is small. When the cylinder starts changing its orientation there are occasions when it comes close to, or even touches, one of the side walls. If one end of the cylinder comes into in contact with a side wall, that experiment is discarded.

3 Dimensional Analysis

To generalize the conditions and results obtained in this study, they are specified and presented mostly in dimensionless form. The hollow cylinders have three length scales: outer diameter d_o, inner diameter d_i, and length l, so that there are two independents, for which l/d_o and d_i/d_o were taken. The solid/liquid density ratio is $\gamma = \rho_s/\rho_l$. The Archimedes number expresses the relative effects of gravity and viscosity in the sedimentation process. For a particle with a single length scale, e.g., a sphere with diameter d, a common definition of the Archimedes number is $Ar = (\gamma - 1)d^3g/\nu^2$ with g the acceleration due to gravity and ν the kinematic viscosity. Under highly viscous (i.e., Stokes flow) conditions the settling velocity of the sphere is proportional to $(\gamma - 1)d^2g/\nu$, so that the Archimedes number can be interpreted as a Reynolds number. For the hollow cylinders the following definition of the Archimedes number was adopted: $Ar = (\gamma - 1)\left(d_o^2 - d_i^2\right)d_o g/\nu^2$ with the reasoning that the velocity of a horizontally settling hollow cylinder is proportional to $(\gamma - 1)\left(d_o^2 - d_i^2\right)g/\nu$ (the length l to a fair approximation cancels given that drag and net gravity are both proportional to l). Taking d_o as the length scale in the Reynolds number (and thus Archimedes number) leads to the above expression for Ar.

If a cylinder—at least a solid one—is vertically released in a Newtonian fluid it will eventually change its orientation to horizontal [17]. The timescales over which this happens and whether it happens in a monotonic or a wobbling way depend on the Archimedes number and the aspect ratio(s) [12]. As in our previous paper [17], we characterize this process by measuring two dimensionless parameters. The first is the dimensionless time t_m at which the cylinder reaches a horizontal orientation (i.e., $\theta = 0$) for the first time: $t_m = t_h \nu / d_o^2$ with t_h the dimensional, measured time (in seconds); the relative uncertainty of t_h for repeated experiments is about 5.6 %. The second is the Reynolds number at the moment $t = t_h$: $Re = |U| d_o/\nu$, with $|U|$ the absolute value of the vertical velocity of the center of the cylinder at that moment.

In order to determine $|U|$, the image frames close to the moment the cylinder becomes horizontal for the first time must be analyzed. Two image frames n and m, before and after the moment at which $\theta = 0$, respectively, are selected, with $2 \leq |m-n| \leq 5$ and the vertical distance traveled by the cylinder's center of mass δs is determined. Then $|U| = \delta s/\delta t$ with $\delta t = |m-n|/f$. The uncertainty in δs mainly comes from the size of the pixels, and is estimated to be 1–2 pixels. This leads to a worst-case relative error in $|U|$ of approximately 10 %.

Each experiment is repeated at least three times and the values reported (dimensionless velocities and times to horizontal) are the averages of the multiple realizations. The error bars presented are the standard deviations of the averages.

4 Simulations Setup

We have performed three-dimensional, time-dependent, particle-resolved simulations to compare with the experimental data and to enhance our understanding of the fluid flow phenomena associated with the settling of hollow cylinders. As in our previous paper on settling cylinders [17], the lattice Boltzmann (LB) method was used for solving the fluid flow. In the LB method, the flow variables are represented by velocity distribution functions that satisfy a discrete version of the Boltzmann equation [18, 19]. This equation is solved numerically on a cubic lattice with spacing Δ and evolved in time with a time step Δt. The velocity distributions are defined in the center point ("node") of each cubic cell, and from the distributions the fluid velocity and pressure are derived [20].

At the surface of the (hollow) cylinder, a no-slip condition is imposed through an immersed boundary (IB) method [21]. For this, the surface is defined by a set of closely spaced points (nearest-neighbor spacing ~0.5Δ). These off-lattice points are called marker points. At each marker point the fluid velocity is determined on the basis of trilinear interpolation from the lattice nodes and then compared with the solid velocity at that marker point, which is known given the linear and angular velocity of the cylinder and the location of the marker point relative to the center location of the cylinder. If the two velocities (fluid and solid) are different, a force is exerted on the fluid that drives this velocity difference to zero, thereby achieving no-slip [22].

Integrating the force distribution over the surface of the cylinder gives the overall force and torque exerted by the fluid on the cylinder. These are used to update the cylinder's linear and angular velocity. A split-derivative algorithm is used to integrate Newton's second law (linear motion) and Euler's equations (rotation) in time with a time step Δt that is the same as the LB time step. Finally, the location and orientation of the cylinder are updated. For the latter a quaternion [23] has been used.

The default spatial resolution of the simulations is such that the outer cylinder diameter spans 12 lattice spacings: $d_o/\Delta = 12$. In previous work [17] it was shown that simulations with higher resolution ($d_o/\Delta = 16$) under the same physical conditions closely matched those with the lower resolution of 12. Also, in the current paper such comparisons have been made to establish the effect of spatial resolution for hollow cylinders. The default time step is such that $\Delta t = 7.7 \times 10^{-4} \sqrt{d_o/g}$.

The simulation domain is periodic in all three coordinate directions. This is because it is computationally not feasible to simulate the entire experimental column (see also the discussion on this topic in [17]). The default domain size in the three Cartesian coordinate directions is $nx \cdot ny \cdot nz = 12.5 d_o \cdot 5 d_o \cdot 150 d_o$. With gravity acting in the negative z-direction ($\mathbf{g} = -g\mathbf{e}_z$) a tall domain is needed to properly capture the wake behind the cylinder. The hollow cylinder is released fully submerged in still liquid, oriented with an angle that deviates 0.5° from fully vertical and with zero velocity; this is done to mimic the angle uncertainty at release in the experiment. The initial slight inclination angle means that if the cylinder rotates it will do so around the y-axis so that the domain size in the y-direction can be made relatively small, which is helpful for limiting computational time. In our previous work on solid cylinders [17] we have shown that the release angle has only limited effect on the settling process of the cylinder.

5 Results

5.1 The Flipping Process

Fig. 1 shows how the settling process of the cylinders was visualized and subsequently analyzed. Zero time corresponds to the moment the cylinder was released with vertical orientation. Over time the cylinder rotates to eventually achieve a horizontal orientation. At the relatively low Archimedes number ($Ar = 4.95$) in Fig. 1 the horizontal orientation is reached monotonically, i.e., the cylinder does not wobble. The camera frames were analyzed so as to determine the vertical location (z) of the end points of the cylinder. The vertical distance between the end points Δz and the length of the cylinder l allow for determination of the angle θ between the cylinder and the horizontal plane: $\theta = \arcsin(\Delta z/l)$. A time series of θ is shown in Fig. 1b.

At higher Archimedes numbers the flipping to horizontal is much faster when measured in dimensionless time ($t\nu/d_o^2$) and ceases to be monotonic. Fig. 2 shows the same hollow cylinder as used in Fig. 1, but now it is falling through less viscous liquids (*m2* and *m9*; see Tab. S1 of the Supporting Information) and thus at higher Ar. When reaching $\theta = 0$ for the first time the cylinder now continues its rotation and enters a wobbling state. The duration of this state, measured as the number of

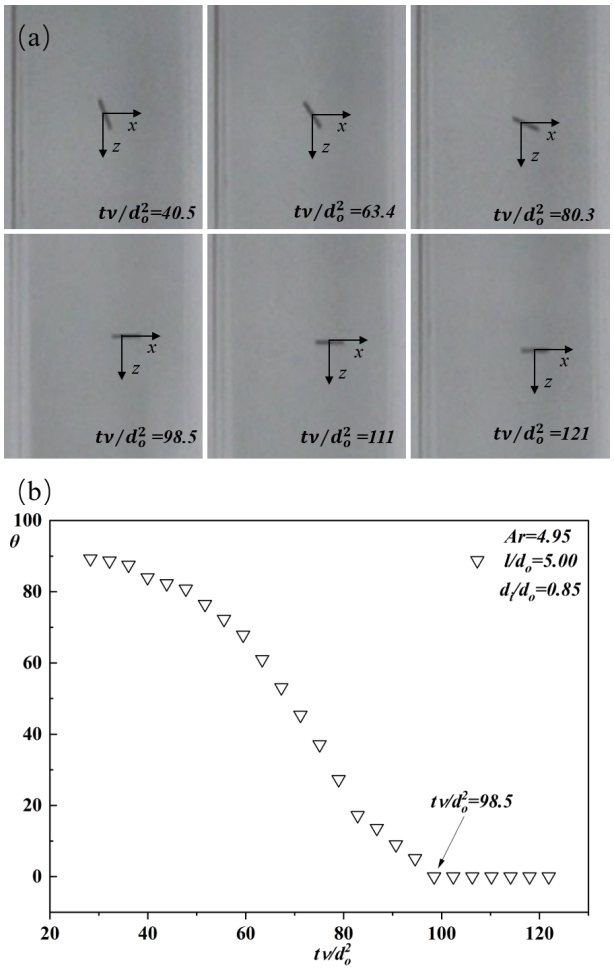

Figure 1. (a) Sample camera frames of a settling experiment recorded at $f = 100\,s^{-1}$ for a hollow cylinder with $d_i/d_o = 0.85$ and $l/d_o = 5.00$ falling through a glycerol-water mixture ($Ar = 4.95$). (b) Time series of the angle θ of the hollow cylinder with the horizontal plane.

wobble periods, and the amplitude of wobbling both increase with increasing Archimedes number (cf. left and right parts of Fig. 2).

In Fig. 3 the flipping process is compared between cylinders falling though liquid mixture *m1* with the cylinders having the same length l and outer diameter d_o but different inner diameters d_i. Clearly, increasing d_i results in slowing of the flipping process, not only in dimensionless time tv/d_o^2 but also in real time, given that d_o and ν are the same for all cases shown in Fig. 3. Given the definition $Ar = (\gamma - 1)\left(d_o^2 - d_i^2\right)d_o g/\nu^2$, an increase in d_i means a decrease in *Ar*. Therefore, observations in Fig. 3 can be interpreted as an increase in flipping time with a decrease in Archimedes number, which fits with the trend observed in our previous study on solid cylinders [17].

Figs. 4 and 5 show the vertical-to-horizontal flipping process as represented by the simulations, including checks on sensitivity to numerical parameters. Fig. 4 is a qualitative impression in which not only the cylinder but also the flow field that is generated by the cylinder falling through the liquid is shown. The cylinder creates a very long wake behind it, which is the reason why a tall simulation domain is needed. Fig. 4a shows the cylinder from above. The liquid inside the cylinder has a speed comparable with that at the outer diameter of the cylinder, i.e., the liquid inside the cylinder largely moves with the cylinder. The flow through the cylinder during its sedimentation is examined in more detail below. Fig. 4c is an illustration of the periodic boundary conditions, in this case in the *x*-direction; looking up from the cylinder, the wake here crosses the left boundary of the flow domain ($x = 0$) to continue at the right side with $x = 12.5d_o$. At the moment shown in Fig. 4d the cylinder has completed the flipping process.

Fig. 5 shows time series of the orientation angle θ and $Re = |u_z|\,d_o/\nu$ (the Reynolds number based on the instantaneous vertical velocity of the center of mass of the cylinder) derived from the simulations. The left panels show the effect of the spatial resolution of the simulation on the behavior of the cylinder. A simulation for which d_o spans 16 lattice spacings Δ is compared with one having $d_o = 12\Delta$. Only minor differences are observed, so it is concluded that a resolution of $d_o = 12\Delta$ is reasonable. In the middle two panels a hollow cylinder and a solid cylinder with the same l/d_o and the same *Ar*. This result supports our definition of *Ar*, given that the two cylinders behave comparably in terms of the timescales of flipping and the associated Reynolds number. It means that the behavior of a hollow cylinder is similar to that of a solid cylinder having the same *Ar* and l/d_o. The right panels of Fig. 5 deal with the effect of the l/d_o aspect ratio. They demonstrate that—also for hollow cylinders—the dynamics of flipping is faster for shorter cylinders, whereas the eventual settling Reynolds number is more or less independent of l/d_o. The latter is because both drag and net gravity are approximately linear functions of *l*.

The simulations allow for a detailed analysis of the flow phenomena associated with the cylinder moving through liquid. Given that hollow particles are used in practical applications for enhancement of transfer processes, it is worthwhile to monitor the flow rate inside a hollow cylinder. For this the average axial velocity $\langle u \rangle$ of the liquid relative to the cylinder was determined. A sample result of how $\langle u \rangle$ is correlated with the flipping process is shown in Fig. 6. Orientation and speed of the cylinder determine the strength of the flow through the cylinder. Upon vertical release the through-flow rapidly increases. After reaching a maximum value of $\langle u \rangle d_i/\nu \approx 2.8$ the through-flow gets weaker as a result of the combined effect of rotation of the cylinder and slowing down of the cylinder. Given that Fig. 6 deals with a wobbling cylinder, flow reversal is observed inside the cylinder, i.e., $\langle u \rangle$ changes sign, approximately at the same moment when the cylinder becomes horizontal for the first time (at $tv/d_o^2 = 1.2$). Note that the Reynolds number associated with the through-flow is one to two orders of magnitude smaller than that associated with the settling process.

5.2 Dependencies on the Archimedes Number

Herein the effect of the Archimedes number on the settling behavior of hollow cylinders is characterized by two metrics: (1) the dimensionless time tv/d_o^2 for the cylinder to complete a 90° rotation; (2) the Reynolds number at that moment. Results

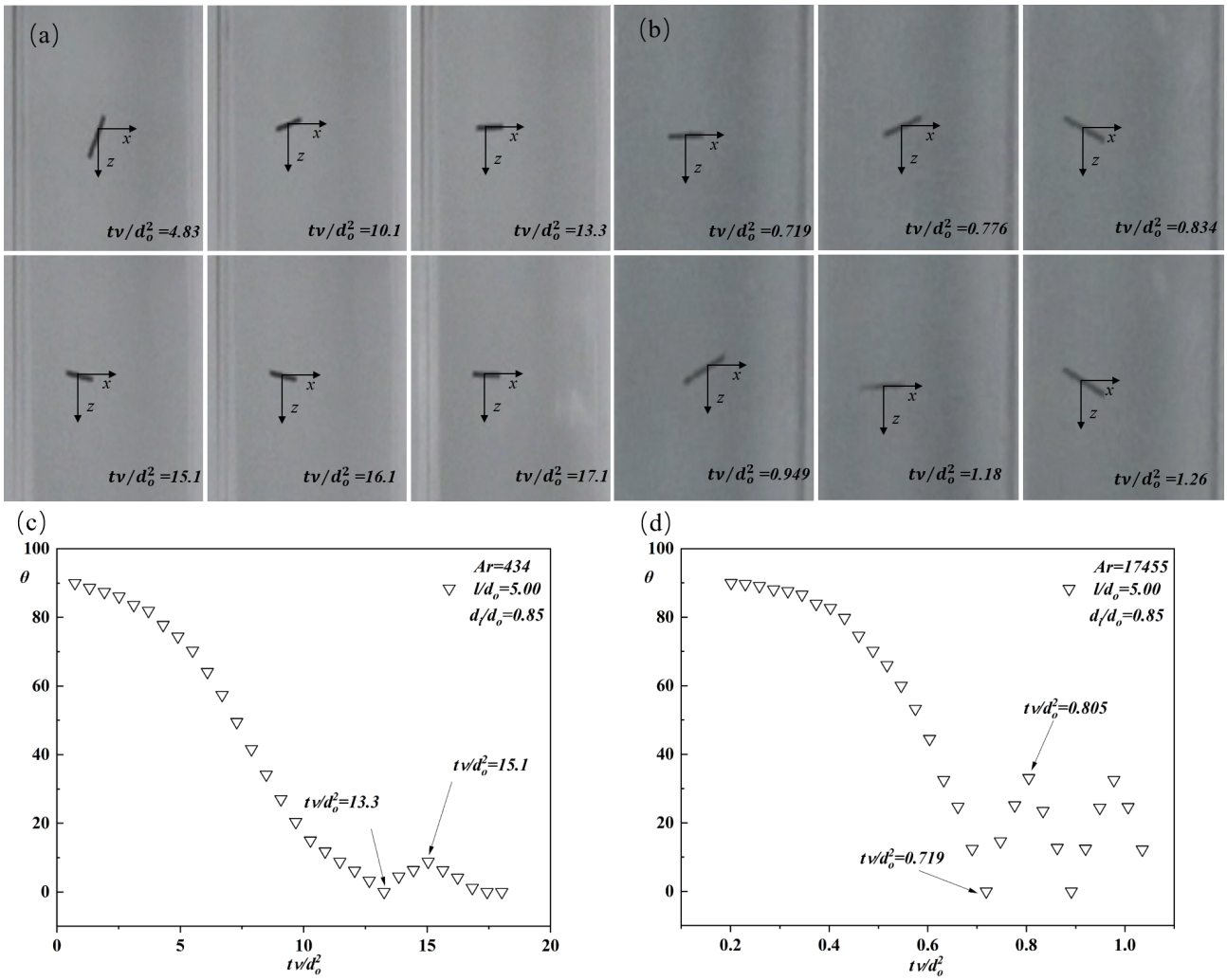

Figure 2. Impressions of the flipping process and how it depends on *Ar*. Image frames and corresponding θ time series. In (a) and (c), Ar = 434. In (b) and (d), Ar = 17455. The cylinder is the same, with l/d_o = 5.00 and d_i/d_o = 0.85; the difference in Ar is due to different viscosities.

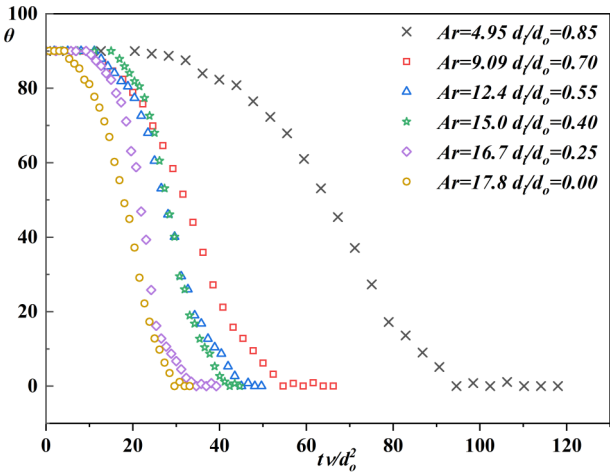

Figure 3. Time series of the angle θ of the cylinder with the horizontal plane for various d_i/d_o at l/d_o = 5.00. The variation of the Archimedes number is due to the variation of d_i/d_o.

for tv/d_o^2 are shown in Fig. 7 for different l/d_o aspect ratios. The overall trend is clear: the cylinder flips faster with increasing *Ar*. For $Ar > 10$, the slope in Fig. 7 is approximately –0.6 so that, given the double-logarithmic scales, $tv/d_o^2 \propto Ar^{-0.6}$. Data points that have different d_i/d_o are on the same trend line. This then means that with the definition of the Archimedes number as $Ar = (\gamma - 1)(d_o^2 - d_i^2)d_o g/\nu^2$ the flipping behavior of hollow and solid cylinders alike can be captured, i.e., this definition of the Archimedes number encompasses the effect of d_i/d_o. If the trend lines are written as $tv/d_o^2 \propto Ar^{-0.6}$ the prefactor χ depends on l/d_o. Fitting the experimental data points for $Ar > 10$ gives χ values of 44, 57, 100, and 132 for l/d_o values of 2.50, 5.00, 7.50, and 10.0, respectively. This shows, as expected, an increased flipping time for longer cylinders.

Fig. 7 also shows simulation data (only for $l/d_o \approx 7.5$ and 10). For $Ar > 100$ simulation results and experiments agree well. For smaller *Ar*, the flipping time is overestimated by the simulations. This might be due to the limits that were imposed on the simulation domain size for computational reasons. These

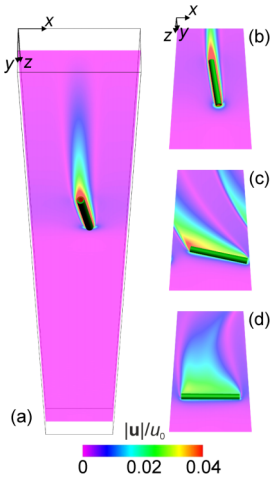

Figure 4. Impressions of a simulation at $Ar = 2057$ with $l/d_o = 9.34$ and $d_i/d_o = 0.625$. (a) Overall view of simulation domain at moment $tv/d_o^2 = 0.59$; (b) detailed view at the same moment; (c) and (d) detailed views at $tv/d_o^2 = 1.18$ and 2.36, respectively. In the color scale $u_o = (\gamma - 1)gd_o^2/\nu$.

limits are mostly felt for low *Ar*, as then the presence of the cylinder is felt over a larger volume of fluid surrounding the cylinder.

Fig. 8 shows the Reynolds number based on the vertical velocity of the center of mass of the cylinder at the moment it becomes horizontal for the first time for different l/d_o. As in Fig. 7, the experimental data points in Fig. 8 for different values of d_i/d_o lie approximately on the same trend line, again supporting our *Ar* definition. It also is observed that the Reynolds numbers are hardly sensitive to l/d_o. This can be understood given that for a horizontal cylinder the drag force on a cylinder

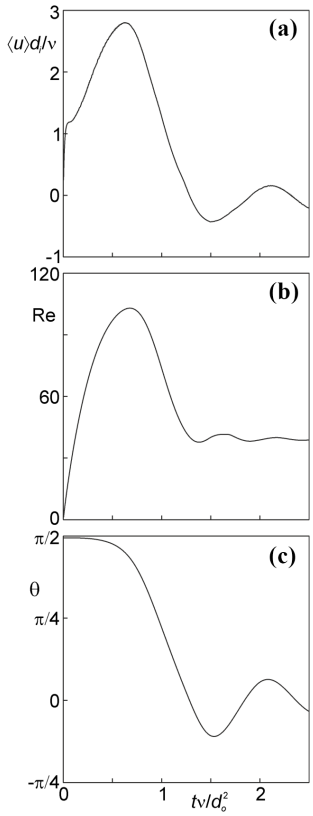

Figure 6. Time series of the average velocity $\langle u \rangle$ (made dimensionless by ν/d_i) of the flow through the settling cylinder (a). Correlation of this through-flow with *Re* (b) and θ (c). $Ar = 2057$, $l/d_o = 9.34$ and $d_i/d_o = 0.625$.

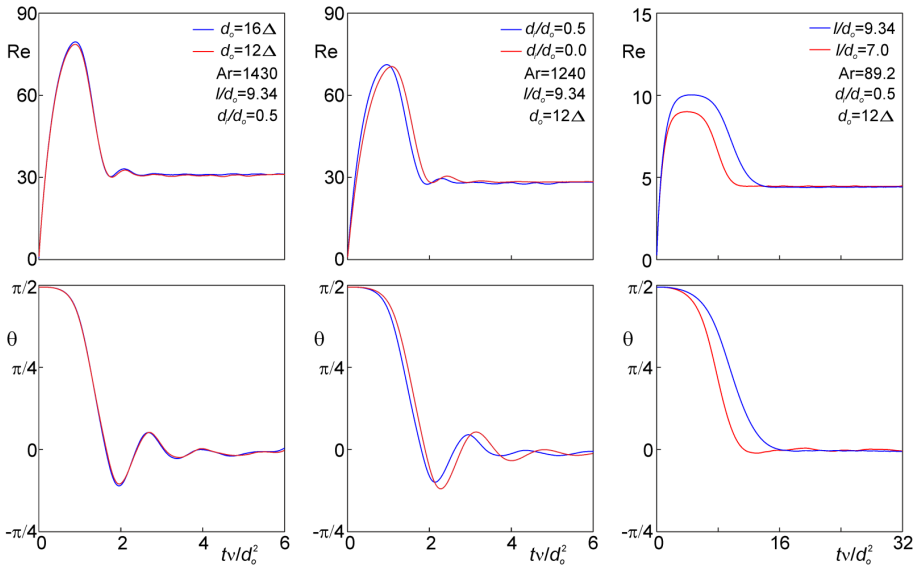

Figure 5. Simulated time series of *Re* (top) and θ (bottom). Left: comparison between two spatial resolutions ($d_o = 16\Delta$ and $d_o = 12\Delta$) at *Ar* and aspect ratios l/d_o and d_i/d_o as indicated. Middle: comparison between a hollow cylinder ($d_i/d_o = 0.5$) and a massive cylinder ($d_i/d_o = 0$) at the same *Ar* and l/d_o. Right: effect of l/d_o (9.34 versus 7.0) under the indicated conditions.

to a good approximation is proportional to its length. With net gravity also proportional to length, this leads to a settling speed that is not (strongly) dependent on the cylinder's length. The simulation results in terms of Reynolds number are in good agreement with experimental data.

6 Conclusion

This paper reports on settling of hollow cylinders in a Newtonian liquid. The emphasis of the work is on quantitative visualization experiments; it is supported by particle-resolved numerical simulations. A central hypothesis of the paper is that it is feasible to correlate the behavior of solid and hollow cylinders with a single *Ar* value, the expression of which incorporates

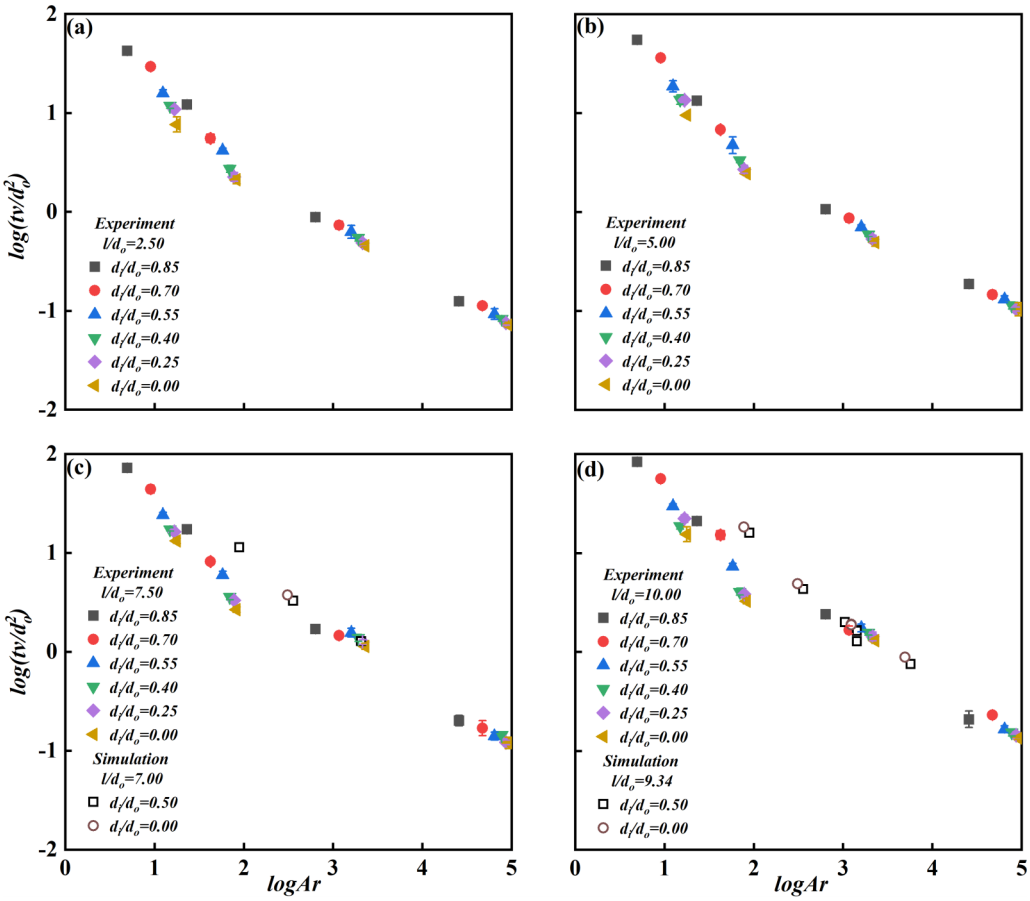

Figure 7. Dimensionless time to reaching a horizontal orientation for the first time (tv/d_o^2) versus *Ar* for l/d_o ratios of 2.50 (a), 5.00 (b), 7.50, and 10.0 (d). Variations of the Archimedes number are due to variations in viscosity and in d_i/d_o.

the outer diameter and inner diameter (zero for solid cylinders). The metrics used for characterizing the sedimentation process are the time it takes for a vertically released cylinder to reach a horizontal orientation for the first time and the Reynolds number at that moment. The proposed expression for the Archimedes number reads $Ar = (\gamma - 1)(d_o^2 - d_i^2)d_o g/\nu^2$; it has been argued that Archimedes number is proportional to the Reynolds number based on the settling speed of a horizontal cylinder.

The experimental data show that the Reynolds number at the moment the cylinder becomes horizontal for the first time is indeed to a good approximation uniquely dependent on *Ar*, i.e., it hardly depends on l/d_o or d_i/d_o. The dimensionless time to horizontal orientation tv/d_o^2 depends on *Ar* and l/d_o, but hardly on d_i/d_o.

The numerical simulations described in this paper serve a few purposes. First, they provide more detail of the flow in the wake of the settling cylinder. Second, they allow for more rigorous tests of the above-mentioned hypothesis by comparing results for cylinders with different d_i/d_o having exactly the same *Ar* and l/d_o. Settling behaviors of those cylinders closely match. Third, given that the simulations fully represent the cylinder geometry, they allow the flow through the hollow cylinder during sedimentation to be assessed. The Reynolds number of the through flow is one to two orders of magnitude smaller than that of the external flow. Computational limitations mean that the entire experimental flow domain cannot be simulated. In comparing experimental and simulation results, domain size effects particularly show for the smaller *Ar* values, where the simulations tend to overestimate the dimensionless time for rotation to horizontal.

Supporting Information

Supporting Information for this article can be found under DOI: https://doi.org/10.1002/ceat.202300285.

Acknowledgment

This work was supported by the National Natural Science Foundation of China (grant numbers: 22078191, 21978165, 22081340412, and 92156020).

The authors have declared no conflict of interest.

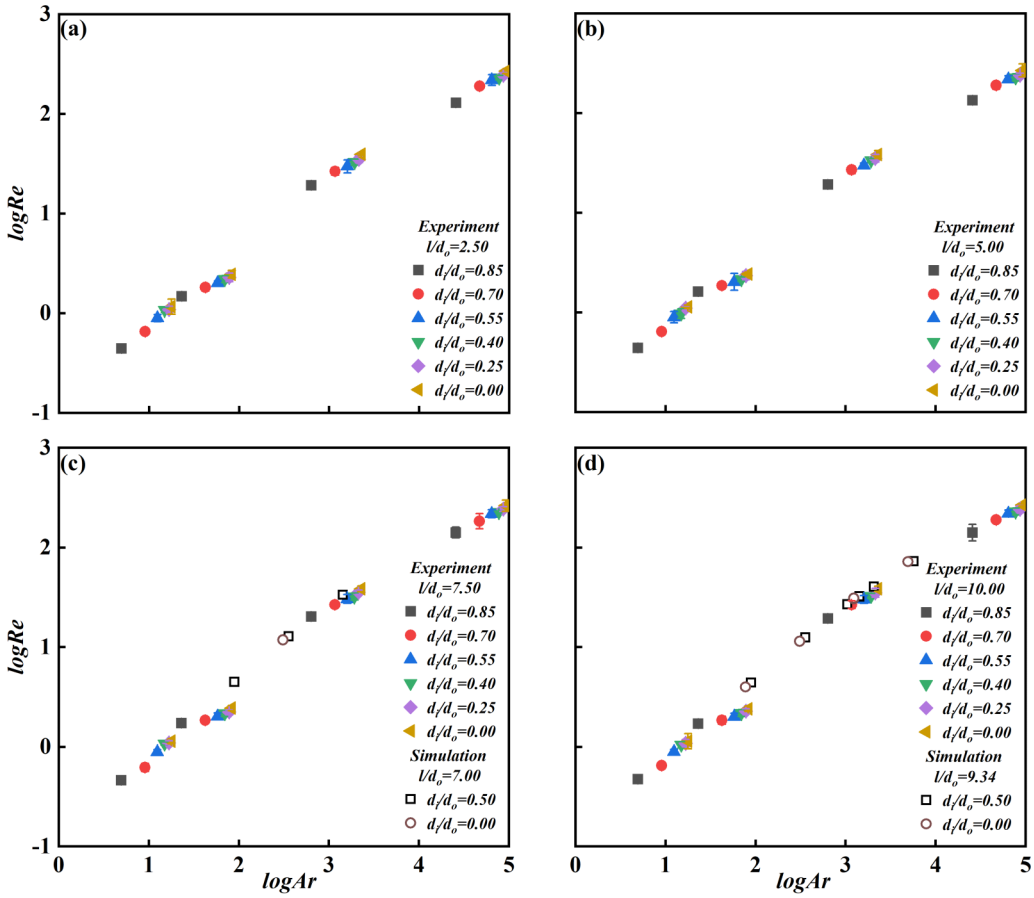

Figure 8. Reynolds number at the moment of reaching horizontal orientation for the first time versus *Ar* for l/d_o ratios of 2.50 (a), 5.00 (b), 7.50 (c), and 10.0 (d). Variations of the Archimedes number are due to variations in viscosity and in d_i/d_o.

Symbols used

Ar	[–]	Archimedes number
d	[mm]	diameter
f	[s^{-1}]	frame rate
g	[$m\,s^{-2}$]	acceleration due to gravity
l	[mm]	length
m, n	[–]	image frames
$nx \cdot ny \cdot nz$	[mm]	default domain size in the three Cartesian coordinate directions
Re	[–]	Reynolds number when the cylinder first reaches horizontal orientation
t	[s]	time
u	[$m\,s^{-1}$]	velocity
$\langle u \rangle$	[$m\,s^{-1}$]	average axial velocity in the cylinder
$\lvert U \rvert$	[$m\,s^{-1}$]	absolute value of the vertical velocity of the of the cylinder at that moment it becomes horizontal

Greek letters

γ	[–]	solid/liquid density ratio
Δ	[–]	lattice spacing
Δt	[s]	time step
Δz	[m]	vertical distance between the end points
δ	[mm]	pixel square size
δs	[m]	vertical distance traveled by the cylinder's center of mass
δt	[s]	time required to shift by the cylinder's center of mass
θ	[–]	angle between cylinder and the horizontal plane
ν	[$m^2 s^{-1}$]	kinematic viscosity
ρ	[$g\,cm^{-3}$]	density
χ	[–]	prefactor

Sub- and superscripts

h	horizontal
i	inner
l	liquid
m	dimensionless
o	outer
s	solid
z	vertical

Abbreviations

IB	immersed boundary
LB	lattice Boltzmann
PRS	particle-resolved simulation

References

[1] L. D. Wit, C. V. Rhee, A. Talmon, *Environ. Fluid Mech.* **2015**, *15 (1)*, 41–66. DOI: https://doi.org/10.1007/s10652-014-9357-0

[2] G. Fromant, D. Hurther, J. Zanden, D. A. A, I. Caceres, T. O'Donoghue, J. S. Ribberink, *J. Geophys. Res. C: Oceans* **2019**, *124 (1)*, 75–98. DOI: https://doi.org/10.1029/2018jc014406

[3] N. G. Deen, M. V. S. Annaland, J. A. M. Kuipers, *Chem. Eng. Sci.* **2004**, *59 (8-9)*, 1853–1861. DOI: https://doi.org/10.1016/j.ces.2004.01.038

[4] L. Q. Lu, J. Yu, X. Gao, Y. P. Xu, M. Shahnam, W. A. Rogers, *AlChE J.* **2020**, *66 (6)*, 1–10. DOI: https://doi.org/10.1002/aic.16969

[5] D. Alfonso, C. Perpiñá, A. Pérez-Navarro, E. Peñalvo, C. Vargas, R. Cárdenas, *Biomass Bioenergy* **2009**, *33 (8)*, 1070–1079. DOI: https://doi.org/10.1016/j.biombioe.2009.04.002

[6] X. K. Lu, A. Bertei, D. P. Finegan, C. Tan, S. R. Daemi, J. S. Weaving, K. B. O'Regan, T. M. M. Heenan, G. Hinds, E. Kendrick, D. J. L. Brett, P. R. Shearing, *Nat. Commun.* **2020**, *11 (1)*, 2079. DOI: https://doi.org/10.1038/s41467-020-15811-x

[7] A. Andersson, J. Holmberg, R. Haggblad, *Top. Catal.* **2016**, *59 (17–18)*, 1589–1599. DOI: https://doi.org/10.1007/s11244-016-0680-1

[8] B. Partopour, A. G. Dixon, *AlChE J.* **2020**, *66 (5)*, 1–13. DOI: https://doi.org/10.1002/aic.16904

[9] S. Movahedirad, A. M. Dehkordi, E. A. Molaei, M. Haghi, M. Banaei, J. A. M. Kuipers, *Chem. Eng. Technol.* **2014**, *37 (12)*, 2096–2102. DOI: https://doi.org/10.1002/ceat.201300565

[10] G. E. Stringham, D. B. Simons, H. P. Guy, *U.S. Geol. Surv. Prof. Pap. U.S.* **1969**.

[11] P. D. Komar, C. Reimers, *J. Geol.* **1978**, *86 (2)*, 193–209. DOI: https://doi.org/10.1086/628496

[12] C. Toupoint, P. Ern, V. Roig, *J. Fluid Mech.* **2019**, *866*, 82–111. DOI: https://doi.org/10.1017/jfm.2019.77

[13] Z. H. Cheng, A. Wachs, *J. Comput. Phys.* **2022**, *471*, 111669. DOI: https://doi.org/10.1016/j.jcp.2022.111669

[14] M. Uhlmann, *Phys. Fluids* **2008**, *20 (5)*, 053305. DOI: https://doi.org/10.1063/1.2912459

[15] A. Wachs, L. Girolami, G. Vinay, G. Ferrer, *Powder Technol.* **2012**, *224*, 374–389. DOI: https://doi.org/10.1016/j.powtec.2012.03.023

[16] J. J. Derksen, *AlChE J.* **2023**, *69 (7)*, e18072. DOI: https://doi.org/10.1002/aic.18072

[17] J. H. Xie, L. J. Zhang, M. H. Lu, J. Lu, J. J. Derksen, *Can J Chem Eng* **2022**, *101 (4)*, 2240–2249. DOI: https://doi.org/10.1002/cjce.24544

[18] S. Succi, J. M. Yeomans, *Phys Today* **2002**, *55 (12)*, 58–60. DOI: https://doi.org/10.1063/1.1537916

[19] H. M. Kushwaha, S. K. Sahu, *Chem. Eng. Technol.* **2015**, *38 (2)*, 235–245. DOI: https://doi.org/10.1002/ceat.201400264

[20] T. Kruger, H. Kusumaatmaja, A. Kuzmin, O. Shardt, G. Silva, E. M. Viggen, *The Lattice Boltzmann Method: Principles and Practice*, Springer International Publishing AG Switzerland, **2017**. DOI: https://doi.org/10.1007/978-3-319-44649-3

[21] M. Uhlmann, *J. Comput. Phys.* **2005**, *209 (2)*, 448–476. DOI: https://doi.org/10.1016/j.jcp.2005.03.017

[22] A. ten Cate, C. H. Nieuwstad, J. J. Derksen, H. E. A. Van den Akker, *Phys. Fluids* **2002**, *14 (11)*, 4012–4025. DOI: https://doi.org/10.1063/1.1512918

[23] J. B. Kuipers, *Aeronaut. J.* **1999**, *103 (1021)*, 127–143. DOI: https://doi.org/10.1017/S0001924000065039

